Applied Surface Science 634 (2023) 157627

Contents lists available at ScienceDirect

Applied Surface Science

journal homepage: www.elsevier.com/locate/apsusc

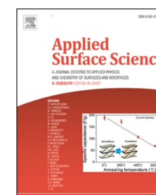

Full Length Article

GaAs hetero-epitaxial layers grown by MOVPE on exactly-oriented and off-cut (1 1 1)Si: Lattice tilt, mosaicity and defects content

Nico Lovergine [a,*], Ilio Miccoli [a,1], Leander Tapfer [b], Paola Prete [c]

[a] Dip. di Ingegneria dell'Innovazione, Università del Salento, Via Monteroni, I-73100 Lecce, Italy
[b] ENEA - National Agency for New Technologies, Energy and Sustainable Economic Development, Brindisi Research Center, Strada Statale 7 'Appia', I-72100 Brindisi, Italy
[c] Istituto per la Microelettronica e Microsistemi del CNR (IMM-CNR), Lecce Unit, Via Monteroni, I-73100 Lecce, Italy

ARTICLE INFO

Keywords:
GaAs heteroepitaxy
Silicon substrate
Rotational twins
Mosaicity
Metalorganic vapor phase epitaxy
X-ray polar figures
High resolution X-ray diffraction
Reciprocal space mapping

ABSTRACT

Integration of III-V devices with Si-photonics and fabrication of monolithic III-V/Si tandem solar cells require the heteroepitaxy of III-V compounds on Si. We report on the lattice tilt, mosaicity and defects content of relaxed GaAs grown by MOVPE on exactly-oriented and 4°-offcut (1 1 1)Si. Thin GaAs single-layers grown at 400 °C and annealed at 700 °C show $\sim 3 \times 10^8$ cm^{-2} density of surface pinholes. Double-layer samples were obtained by GaAs overgrowth at 700 °C. GaAs epilayers are tilted by (0.05–0.14)° with respect to Si. Rotational twins were observed in X-ray diffraction (XRD) pole figures: the most abundant ones originate from 60°-rotation of GaAs around the $[\overline{1}\overline{1}\overline{1}]$ growth direction and are identified as micro-twins along the GaAs/Si hetero-interface. Twins obtained by rotations around the $[\overline{1}\overline{1}1]$, $[1\overline{1}\overline{1}]$, and $[\overline{1}1\overline{1}]$ directions or by combined rotations around the growth direction and one of the former, were also observed. The GaAs mosaicity and block size were studied through high-resolution XRD intensity mapping: for single-layer samples crystal blocks are ascribed to 3–5 nm thin micro-twins, whose size does not change upon annealing. In double-layer samples thicker (32–35 nm) micro-twins occur. GaAs samples grown on offcut (1 1 1)Si show less rotational twins but a reduced mosaic block size with respect to exactly-oriented Si.

1. Introduction

The heteroepitaxy of III-V semiconducting compounds onto Si wafers continues to attract a large research interest due to its pivotal role in the monolithic integration of III-V optoelectronic devices with Si-based photonics [1,2] and fabrication of high-efficiency III-V/Si tandem solar cells [3,4]. However, the direct growth of device-quality III-V heteroepitaxial structures on Si remains difficult due to the combined effects of lattice, thermal and crystal polarity mismatches between III-V compounds and Si. Several types of defects have been observed in III-V/Si heterostructures, including dislocations and stacking faults [3,5,6], twins [5,7,8], anti-phase domains (APDs) [9] and cracks, their occurrence and relative amounts depending on the materials lattice mismatch, substrate orientation and surface preparation, and epitaxial growth conditions. In addition, the surface morphology of as-grown epilayers is heavily affected by the presence of defects and materials nucleation behavior. Common strategies to reduce the amount of defects in III-V/Si structures envisage, among others, adoption of the so-called double-step growth (consisting in the low-temperature – in the range of 400–500 °C – deposition of a thin layer, followed by the high-temperature growth – in the range 600–750 °C – of a thicker epilayer) in combination with (multiple) annealing cycles [6,9], and the use of offcut Si substrates.

Over the last three decades, studies in the field concentrated mostly on the heteroepitaxial growth of III-Vs on (1 0 0)Si [9,10,11], as the latter is the standard wafer utilized in complementary-metal oxide–semiconductor (CMOS) technology. Consequently, alternative substrate orientations has been only seldom explored. However, III-V growth on (1 1 1)-oriented Si has found increasing interest in the last ten years. Indeed, APD-free 3-dimensional GaAs disks were obtained from coalescence of planar nanowires grown by nanoscale selective hetero-epitaxy on V-groove patterned (1 0 0)Si substrates, exposing {1 1 1} crystalline side planes [12]. Low dislocation density and APD-free GaAs micro-ridges on (1 0 0)Si substrates were demonstrated by selective area

* Corresponding author.
E-mail address: nico.lovergine@unisalento.it (N. Lovergine).
[1] Present address: Aixtron SE, Dornkaulstraße 2, D-52134 Herzogenrath, Germany.

https://doi.org/10.1016/j.apsusc.2023.157627
Received 3 April 2023; Received in revised form 4 May 2023; Accepted 26 May 2023
Available online 29 May 2023
0169-4332/© 2023 The Authors. Published by Elsevier B.V. This is an open access article under the CC BY license (http://creativecommons.org/licenses/by/4.0/).

heteroepitaxial growth within flat-bottom trapezoidal-shaped Si pockets bound by {1 1 1} micro-planes [2], a result of the combination of geometrical constraints and specific III-V nucleation onto the (1 1 1)-oriented side facets of the groove. Similar results were obtained for the growth of InP micro-ridges on V-grooved (1 0 0)Si [13], although higher densities of TDs and micro-twins were reported in such case due to the (1 1 1)-nucleation of InP. These findings indicate the technological interest in studying and exploiting the nucleation behavior and defects generation of III-V materials on (1 1 1)Si planes, as such crystal orientation consistently leads to APD-free III-V epilayers on Si and much smoother layer morphology [10].

In addition, (1 1 1)-oriented substrates constitute the preferred template for the self-assembled growth of III-V nanowires. The latter have applications to a variety of novel nanophotonic devices, including low-threshold nano-lasers [14], fast and polarization sensitive photodetectors [15,16] and efficient solar cells [17,18]. As an example, GaAs – AlGaAs core–shell nanowires [19,39] have potentials for vertically integrated nano-laser sources on a Si platform [20]. Also, the growth of nanowires on (1 1 1)Si in substitution of III-V substrates is desirable for the low-cost application of nanowires to photovoltaics. In both cases the deposition of thin (1 1 1)B-oriented III–V buffer layers would ensure good control over the nanowire vertical alignment [21,22,23] and prevent Si doping of as-grown nanowires [24].

The direct heteropitaxy of III-Vs on (1 1 1)Si substrates has been reported for GaP [7], InP [23], GaAs [5,21,22,25,26], and AlSb [27] grown by molecular beam (MBE) or metalorganic vapor phase (MOVPE) epitaxy, by employing the double-step growth approach in combination with various materials annealing processes. However, studies often lack quantitative and statistically sound evaluation of the epilayer defects content and/or mosaicity (block size and tilt) in correlation with actual growth (e.g., initial nucleation) and annealing conditions. Moreover, the heteroepitaxy on offcut (1 1 1)Si substrates has been only seldom studied.

It has been previously demonstrated that, as result of the III-V and Si surface and interface energies, Volmer-Weber (3-dimensional) growth is generally expected during early nucleation stages of III-V/Si heteroepitaxy, including growth on (1 1 1)Si [28]. We recently reported on the low-temperature MOVPE of GaAs by the Volmer-Weber nucleation mechanism on As-stabilized (1 1 1)Si substrates [29]. GaAs nanoisland density, shape, size evolution and coalescence until full coverage of the Si surface was studied in details, as preliminary step towards the heteroepitaxy of GaAs on Si. Building upon these results, here we present the structural properties of GaAs epilayers double-step grown and annealed on both exactly-oriented and offcut (1 1 1)Si substrates. The GaAs lattice tilt (with respect to Si), strain, mosaicity and defects content, with emphasis on the types and relative amounts of rotational twin domains, occurring within the samples were investigated. To this purpose, field-emission scanning electron microscopy (FESEM) observations and X-ray diffraction (XRD) pole figures, along with double- (DA) and triple-axis (TA) XRD measurements were performed on the GaAs/Si structures. Quantitative and statistically relevant information has been obtained from these analyses for samples grown on the different Si substrates and after each of the growth/annealing steps, evidencing their effect (if any) on the overall structure of resulting GaAs epilayers.

2. Experimental methods

Thin GaAs epilayers were grown on Si substrates by low (50 mbar) pressure MOVPE in an Aixtron 200RD reactor, using trimethylgallium (Me_3Ga) and *tert*-butylarsine ($^tBuAsH_2$) as Ga and As precursors, respectively. Either exactly-oriented or offcut (4° towards the $[11\overline{2}]$ direction) (1 1 1)Si wafers were employed as substrates. Immediately prior to loading in the reactor chamber the substrates were cleaned in isopropanol vapors for 1 h, etched at room temperature in diluted (5% by volume in d.i. H_2O) HF for 2 min to remove the native surface oxide layer, thoroughly washed in d.i. H_2O, and blown dry under pure N_2. The substrates were then *in-situ* heat-cleaned at 700 °C for 30 min under Pd-purified H_2 and further annealed in a $H_2 + {}^tBuAsH_2$ flow for 10 min. The thermal treatment in As vapor has a two-fold purpose: (i) it lowers the temperature for decomposition of residual oxides left on the Si surface well below that (950 °C) required for annealing under pure H_2, and (ii) it provides an As-stabilized Si surface [10], which leads to the nucleation of (1 1 1)B-oriented GaAs [21,30]; the substrate was finally cooled to the growth temperature under a continuous H_2+$^tBuAsH_2$ flow, so to keep the Si surface under such As-stabilized conditions until growth initiation. We carefully applied these same (in-situ and ex-situ) surface treatments to both types of Si substrates. The reproducibility of substrate preparation can be inferred by the analysis of early nucleation stages (i.e., before coalescence) of GaAs on Si substrates (see below for growth details), in reason of the high sensitivity of III-V nucleation to Si surface conditions [28]. A detailed study of density, shape and size of as-grown nano-islands was reported in ref. [29]: the same results have been consistently obtained for over a dozen samples, demonstrating the good control achieved using the above Si surface processes.

GaAs epilayers were grown via the double-step growth approach [6]: in the first step a GaAs layer (single-layer samples in the following) was grown at 400 °C under a Me_3Ga molar flow of 49 μmol × min^{-1} and a $^tBuAsH_2$:Me_3Ga precursors molar concentration (V:III) ratio of 5:1; the growth was continued for 60 min, e.g. until a nearly full GaAs coverage of the Si surface was obtained. The nominal thickness of such first layer is ~ 42 nm [29]. Subsequently, the sample temperature was raised to 700 °C and a thermal treatment of the samples was performed for 10 min under a H_2 + $^tBuAsH_2$ atmosphere, so to improve the surface morphology and, possibly, the crystalline structure of as-grown GaAs [5]. A second GaAs layer (double-layer samples in the following) was afterwards deposited at 700 °C under a Me_3Ga molar flow of 8.2 μmol × min^{-1} corresponding to a V:III precursors ratio of 30:1, with the aim to obtain a better optical quality material [22] and low carbon contamination. The growth time of the second GaAs layer was varied between 10 and 30 min.

The surface morphology of as-grown and annealed GaAs/(1 1 1)Si structures was studied by FESEM observations using a Zeiss model Sigma VP microscope equipped with a Gemini-1 electron column using a primary electron beam energy of 5–10 keV.

The overall layer/substrate epitaxial relationships and the occurrence of rotational twins within the GaAs were assessed by X-ray diffraction (XRD) analysis in the θ-2θ Bragg-Brentano geometry using a Rigaku D-Max/Ultima$^+$ triple-axis diffractometer equipped with a MPA2000 thin-film attachment stage and a Cu-anode X-ray tube. The formation of twin-defects inside the as-grown samples was investigated by recording X-ray pole figures: in a typical X-ray pole measurement, the GaAs/(1 1 1)Si sample was step-rotated around the sample azimuthal (ϕ) and inclination (ψ) angles within the ranges $0° \leq \phi \leq 180°$ (with $\Delta\phi = 1°$ angular step) and $0° \leq \psi \leq 75°$ (with $\Delta\psi = 0.5°$ angular step), the X-ray detector being kept fixed at $2\theta = 27.3°$ (corresponding to the (1 1 1)GaAs Bragg reflection), and the X-ray scattered intensity collected.

The strain relaxation, lattice tilt and mosaicity of as-grown GaAs epilayers were evaluated by double-crystal XRD measurements. To this purpose a high-resolution X-ray diffractometer (MRD, Panalytical) was used for recording DA XRD patterns. All measurements were carried out using the Cu-K_α radiation ($\lambda = 0.154$ nm), a conventional 3-kW X-ray generator, and employing a four-bounce Ge(2 2 0) Bartels monochromator-collimator with an angular divergence of the X-ray beam of ~ 12 arcsec. TA XRD measurements and reciprocal space mappings (RSMs) were recorded using a two-reflection channel-cut Ge (2 2 0) crystal as analyzer.

In particular, the epilayers strain state was analyzed by double crystal XRD measurements around the symmetric (1 1 1) and asymmetric (5 1 1) and (4 2 2) reciprocal lattice points (rlps) of GaAs for different azimuthal angles ϕ around the surface normal. RSM measurements were performed around the (1 1 1) rlp of Si and GaAs in order to analyze the

coherent and diffuse scattering along the momentum transfers Q_x and Q_z, i.e. the in-plane and out-of-plane scattering signals, respectively. The TA line-scan profiles along Q_x and Q_z were obtained directly from the RSM by extraction of line scans. In few cases, TA line-scans were also measured directly by ω-scans and ω-2θ scans.

3. Results and discussion

Fig. 1 reports the surface morphology of GaAs single-layers as-grown at 400 °C on exactly-oriented (1 1 1)Si substrates and in-situ thermal annealed at 700 °C. While Fig. 1a shows a morphology reminiscent of the GaAs nanoisland nucleation [29], the annealing process strongly improves the epilayer surface (Fig. 1b), leading to a much flatter and smoother morphology; in addition, the surface evidences the formation of large (sub-micrometric) irregular domains separated each-others by curved (few nm deep) boundaries. Interestingly, similar morphologies have been reported for GaP/(1 1 1)Si [7] and GaAs/(1 0 0)Si [9] structures, and ascribed to the formation of rotational twins and APDs, respectively. As APDs are not expected for (1 1 1)-oriented Si substrates, we are led to ascribe the surface morphology in Fig. 1b to the occurrence of rotational twin domains (see discussion below). Twins have been observed within single GaAs nano-islands as well as upon their coalescence [5]; individual GaAs nano-islands are therefore, not necessarily single-phase domains in the same sense Lucci et al. [28] write of anti-phase mono-domains on (1 0 0)Si. Still, upon further growth, neighboring nano-islands could coalesce without forming twin boundaries (TBs), while some others would generate them. TBs may however, be hidden by the kinetic-roughening of the nano-island surface under the high supersaturation conditions associated with the samples low growth temperature, but are evidenced upon annealing due to atomic rearrangement at the epilayer surface.

Furthermore, a relatively dense [(1–3) $\times$ 10^8 cm^{-2}] distribution of pinholes [31] is observed across the GaAs surface after sample annealing; pinhole formation has been associated with threading dislocations (TDs) in lattice-mismatched heteroepitaxial layers [32], suggesting plastic relaxation in our samples. In this respect, we underline that our estimated pinhole density is in agreement with TD densities commonly reported for annealed GaAs epilayers of comparable thickness on Si [6]. Similar results hold also for GaAs epilayers grown on the offcut Si substrates.

Fig. 2 shows the surface morphology of the GaAs deposit after the second layer growth as function of deposition time. Noteworthy, the morphology is characterized by triangular flat-topped hillocks, whose growth and coalescence determines the formation of a continuous film (see Fig. 2c), the latter corresponding to a (double-layer) GaAs thickness of 190–210 nm. The final film appears relatively smooth, but for the seldom appearance of pyramid-shaped hillocks locally protruding out of the epilayer surface in the growth direction.

By comparing the directions normal to the hillock edges with the substrate cleavage edges, it turned out that the former are aligned to the three equivalent ⟨112⟩ in-plane directions of Si. However, the hillocks appear often 60°-rotated to each other around the vertical growth direction, as evidenced in the plan-view micrograph in the inset of Fig. 2a, suggesting the presence of rotational twin defects inside the as-grown GaAs deposit. High densities of twin domains have been previously observed in the case of GaAs hetero-epitaxy on both (1 1 1)- and (1 0 0)-oriented Si substrates [5,33], as result of the polarity mismatch between the two materials. Two types of twin planes may occur in zinc-blende (ZB) GaAs: ortho- and *para*-twins. The *ortho*-twin has Ga–As bonding over the twin plane and is formed by a 60°-rotation of the crystal around a ⟨111⟩ axis. The *para*-twin is instead, a perfect mirror plane with Ga–Ga or As–As bonding over its plane and is formed by a 180° rotation of a crystal volume around an axis parallel to the twin plane; *para*-twins are thus associated to a polarity inversion of the crystal, and in the case of III-V/Si hetero-epitaxy lead to the formation of APDs. The origin of APDs has long been debated in III-V/(1 0 0)Si structures, and it is now generally agreed that their formation is induced by surface-steps of the Si substrate with heights corresponding to an odd number of monolayers [34].

However, the formation of APDs is not favored on (1 1 1)Si [10]; indeed, we previously showed that our GaAs epilayers are (1 1 1)B-oriented everywhere across the GaAs/Si sample [21], ruling out the occurrence of *para*-twins and APDs within the epilayer. On the contrary, rotational twins have a very low nucleation energy and can easily form as result of growth perturbation, e.g. by mismatch stress fields generated at the GaAs/Si hetero-interface or within the epilayer.

To confirm and further investigate the formation of rotational twins inside as-grown samples, X-ray pole measurements were performed on both single- and double-layer GaAs epitaxial samples. Fig. 3(a-c) shows that GaAs deposition on (1 1 1)Si lead to similar X-ray pole figures for both types of samples; however, the X-ray patterns of the sample grown on the offcut Si substrate in Fig. 3b appear slightly vertically shifted and less intense because of the substrate offcut. Interestingly, a series of extra-reflections can be observed in the pole figures of epitaxial samples in comparison with that of a defect-free (1 1 1)GaAs substrate (reported as reference in Fig. 3d). The latter shows only three main diffraction spots, beyond the central pole (at $\psi = 0°$), corresponding to the three equivalent $[\overline{1}11]$, $[\overline{1}1\overline{1}]$, and $[1\overline{1}\overline{1}]$ directions (indicated in the schematics of Fig. 4), tilted by $\psi = 70.5°$ with respect to the central pole and equally separated by an azimuthal rotation angle (ϕ) of 120°. Instead, all as-grown samples show six intense diffraction spots at $\psi = 70.5°$, equally separated by an azimuthal angle of 60°, twelve reflections at $\psi = 56.3°$, along with additional six weaker reflections occurring at $\psi = 38.9°$.

As better explained by the schematics in Fig. 4, the observed extra-

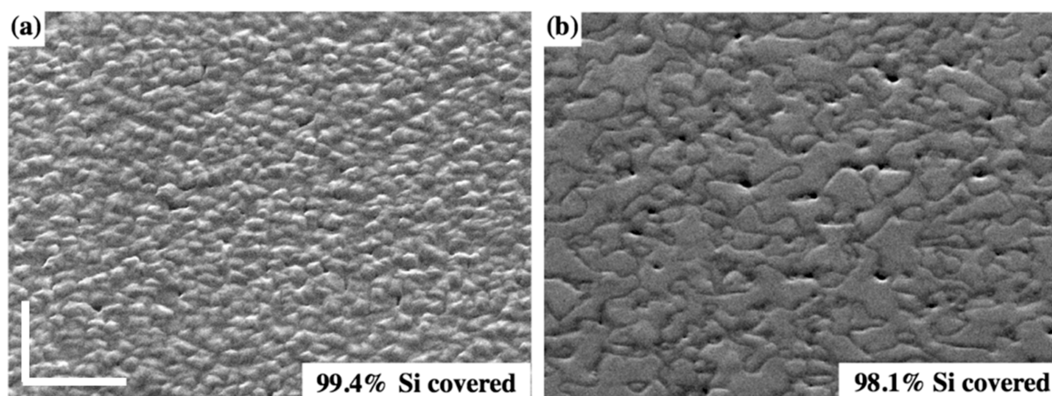

Fig. 1. FE-SEM micrographs (30,000× magnification, 45°-tilt view) of (a) GaAs epilayer grown at 400 °C for 60 min on exactly-oriented (1 1 1)Si substrate, and (b) after annealing at 700 °C for 10 min. White markers in (a) represent 500 nm. Each figure shows the estimated GaAs coverage fraction of Si.

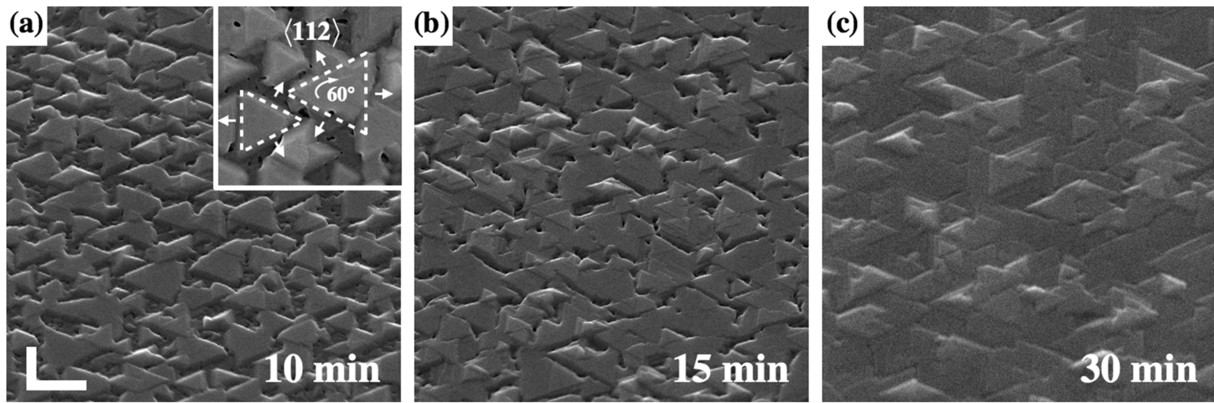

Fig. 2. FESEM micrographs (10,000× magnification, 45° tilt view) showing the surface morphology of double-layer samples, as a function of the second GaAs layer growth time (indicated in the figures). Markers in micrograph (a) represent 1 μm.

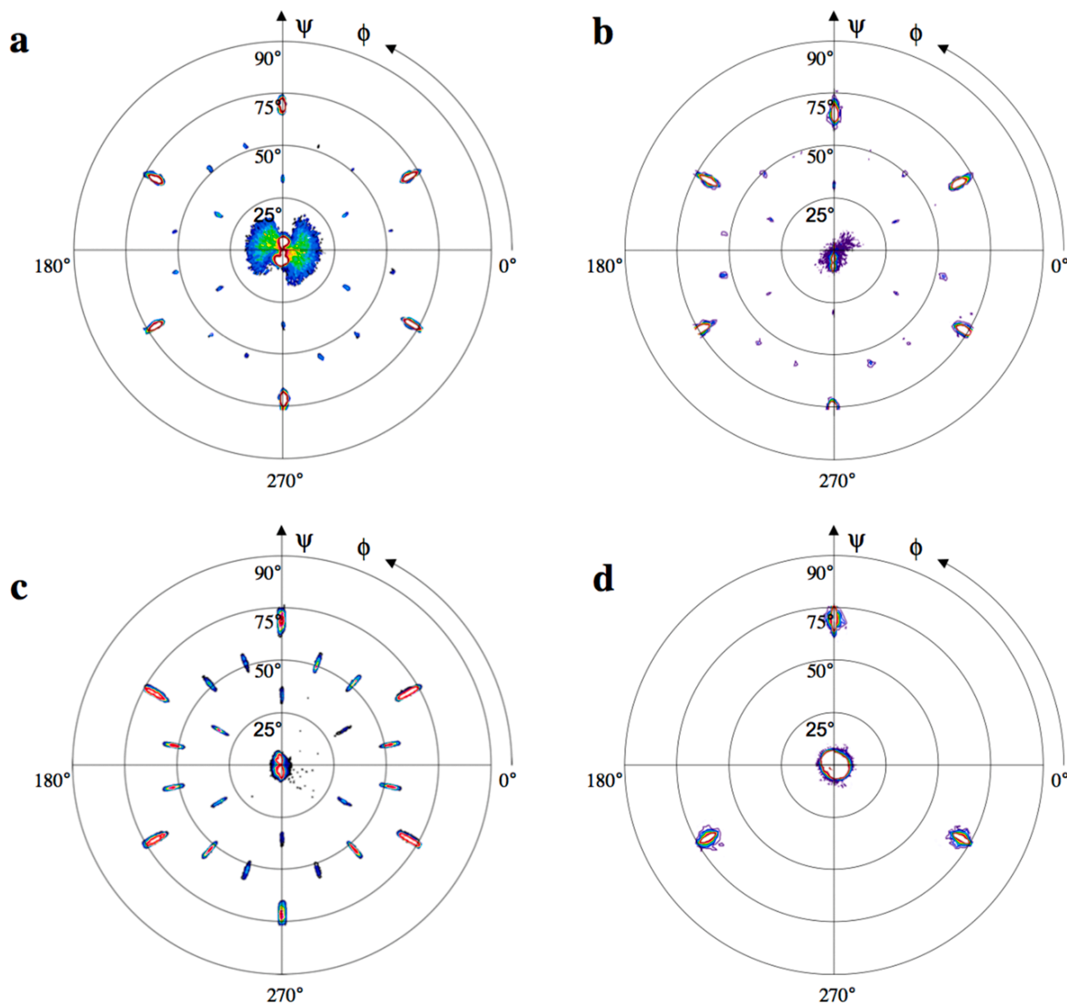

Fig. 3. XRD pole figures of single-layer GaAs grown on (a) exactly-oriented (same sample as in Fig. 1b, and (b) offcut (1 1 1)Si substrates; (c) pole figure of double-layer GaAs on exactly-oriented (1 1 1)Si (same sample as in Fig. 2c); and (d) pole figure of a (1 1 1)B GaAs mono-crystalline wafer.

reflections can be associated to (multiple) rotational twin domains within the as-grown hetero-epitaxial layers, more specifically with the presence of three different families of *ortho*-twin defects, as the following: the first twin family (indicated as A-type in Fig. 4) is formed by a 60°-rotation of the GaAs crystal around the sample $[\overline{1}\overline{1}\overline{1}]$ growth direction and it is associated with the appearance of the three extra-peaks at $\psi = 70.5°$. The second family (indicated as B-type in Fig. 4) is formed by 60°-rotation of the GaAs crystal around each of the three non-vertical $[\overline{1}\overline{1}1]$, $[\overline{1}1\overline{1}]$, and $[1\overline{1}\overline{1}]$ directions and determine the appearance of six extra-peaks at $\psi = 56.3°$ and three extra-peaks at $\psi = 38.9°$. The remaining nine extra-reflections (indicated as AB-type in Fig. 4) are generated upon the application of an additional 60°-rotation around each of the non-vertical equivalent directions (as in B-type twins) to an A-type rotated GaAs crystal domain.

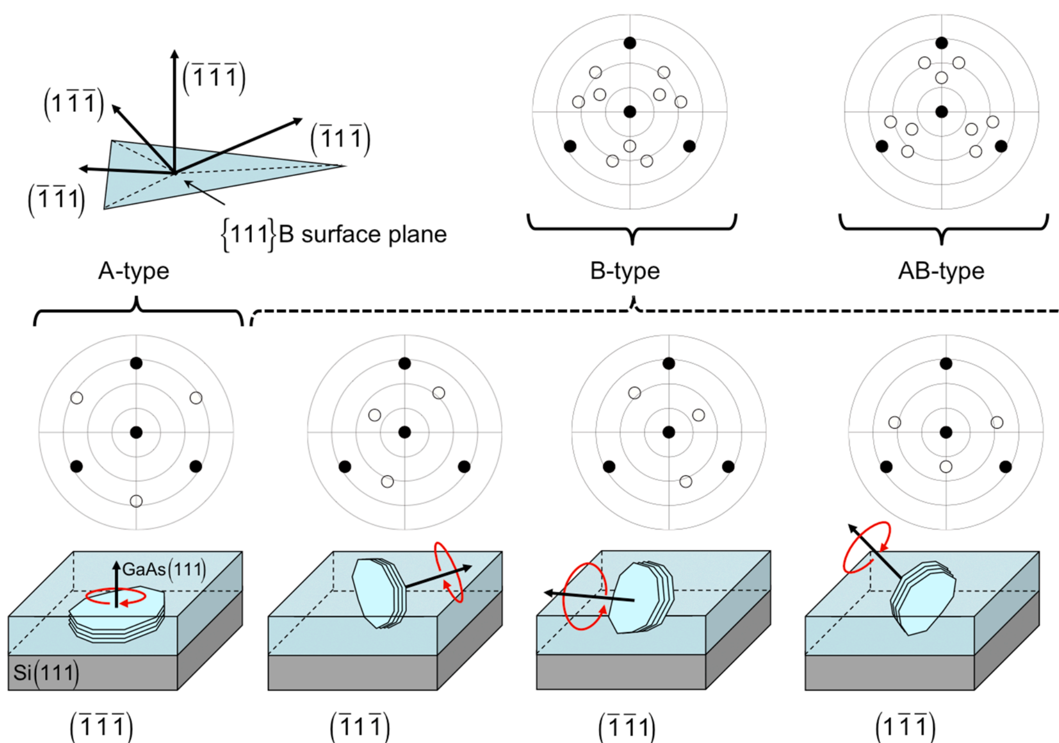

Fig. 4. Schematics of the different *ortho*-twin defects (namely, A-, B- and AB-type) occurring in the as-deposited GaAs epitaxial layers, and associated 60°-degree crystal rotations around various ⟨111⟩ reflections. Black spots in the schematic polar diagrams represent ⟨111⟩ reflections associated to a perfect GaAs crystal. White spots represent additional reflections originated from the A-, B- and AB-type rotational twins, as indicated.

The XRD pole figures further allowed a quantitative estimate of the twin-domains relative volume content in the samples. For GaAs buffer layers grown on exactly-oriented (1 1 1)Si substrates, the adjacent XRD reflections at (ψ_1, ϕ_1)=(70.5°, 90°) and (ψ_2, ϕ_2)=(70.5°, 30°) were considered, being attributed to the A-type twinned and original (untwinned) crystal, respectively. For the off-cut Si substrate samples, the above X-ray peak positions are slightly shifted because of the substrate 4° offcut angle, leading to two reflections at (ψ_1, ϕ_1)=(65.5°, 90°) and (ψ_2, ϕ_2)=(69°, 29°), correspondingly. The intensity profiles of the two peaks were then obtained by plotting the diffracted intensity as function of the sample inclination angle ψ (between 60° and 75°), while keeping fixed the azimuthal angle at $\phi_1 = 90°$ and $\phi_2 = 30°$ ($\phi_2 = 29°$) for the exactly-oriented (off-cut) samples; a plot of the as-obtained intensity profiles for the sample grown on off-cut Si is reported as an example in Fig. 5. Integration of each peak intensity profile allowed to calculate the total diffracted intensities relative to the twinned (I_T) and untwinned (I_{NT}) domain volumes in each sample, from which the relative amount of twinned crystal volume within the GaAs epilayer – the so-called *rotational twin ratio* – was finally estimated as $I_T/(I_T + I_{NT})$.

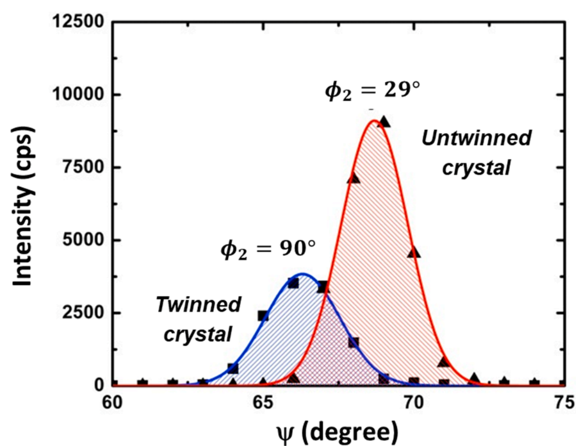

Fig. 5. ψ scans of the diffracted X-ray intensity obtained from the single-layer sample pole pattern in Fig. 3(b), for an azimuthal angle fixed at $\phi_1 = 90°$ (twinned crystal) and $\phi_2 = 29°$ (un-twinned crystal). The solid curves represent the Gaussian line profiles best-fitting the experimental data (solid points).

Noteworthy, the content of A-type twin domains turned out rather high for the single-layer samples grown on exactly-oriented Si, with a rotational twin ratio around (48±1)%, which remains around (45% ±3)% upon deposition of the second GaAs layer. As the XRD peak intensities pertaining to the B- and AB-type twin domains in the pole figures are much weaker than those of A-type ones, a reliable estimate of their relative volumes cannot be performed for the former; therefore, the overall volume content of twinned domains in the present samples is likely not much higher than that estimated for A-type ones. Interestingly, the rotational twin ratio of the latter decreases down to (32±1)% for GaAs epilayers grown on the offcut Si substrates, similar to the case of GaP/(1 1 1)Si [7]. To the best of the authors' knowledge no such figures have been previously reported for GaAs/(1 1 1)Si structures grown by MOVPE. However, for MBE-grown samples on exactly-oriented (1 1 1)Si rotational twin ratios ~ 50% were reported at low V:III ratios [25], i.e. not far from present ones. Rotational twin ratios were further reported to decrease down to 8% with increasing V:III ratios >100.

The strain relaxation (lattice mismatch) between the GaAs layers and the (1 1 1)Si substrate was evaluated by DA diffraction scans. Fig. 6 shows the DA scans around the (1 1 1) and (5 1 1) Bragg reflections of single- and double-layer samples on exactly-oriented Si. The angular distances between the GaAs layer and the Si substrate peaks, $\Delta\theta_{111}$ and $\Delta\theta_{511}$, are the same for both samples, and corresponds to a relaxed GaAs lattice, i.e. to ~ 4% lattice mismatch between GaAs and Si. A second-order approximation for the relationship between lattice strain field and angular distance between Bragg peaks was used for the analysis of experimental data [35].

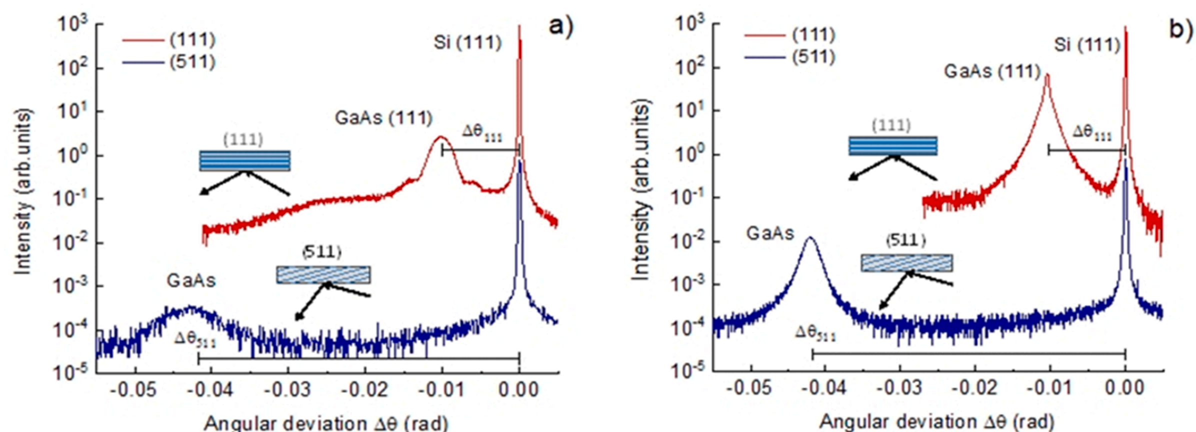

Fig. 6. (a) DA X-ray patterns of single- (a) and a double-layer (b) samples grown on exactly-oriented (1 1 1)Si; the (1 1 1) symmetric (upper curves, red lines) and the asymmetric (5 1 1) diffraction curves in the glancing incident geometrical configuration (lower curves, blue lines) are shown. The angular distances $\Delta\theta_{111}$ and $\Delta\theta_{511}$ between the (1 1 1) and (5 1 1) Bragg peaks of the Si substrate GaAs epilayer respectively, show that the single- and double-layer heterostructures are completely relaxed.

In order to avoid misinterpretations, several DA scans at different azimuthal angles were recorded. These measurements (not shown here) indicate a very small rotation of the GaAs lattice with respect to the Si lattice, i.e. the ⟨1 1 1⟩ GaAs axis is tilted with respect to the ⟨1 1 1⟩ Si axis, and may be caused by the introduction of misfit dislocations at the GaAs–Si interface. The maximum tilt angle measured (which depends on the azimuthal angle) for exactly-oriented Si substrates is about 0.05° for the single-layer sample and 0.08° for the double-layer one. This finding is in agreement with similar observations for GaAs epilayers grown by MBE on (1 0 0)Si, in which tilt angles between 0.05° and 0.17°, depending on the layer thickness (in the 1–4 μm range), were found [36]. Tilt angles of 0.11° and 0.14° were measured respectively, for single- and double-layer samples grown on offcut substrates, i.e. about twice those measured for samples on the exactly-oriented substrates.

Noteworthy, the DA peaks of GaAs show a clear broadening due to lattice defects, the latter induced by the rapid relief of the large lattice mismatch during initial stages of epitaxial growth, and crystal mosaicity. Indeed, the GaAs epilayer can be regarded as constituted by crystal blocks/domains of finite size having slightly different crystal orientations with respect to the main (average) alignment axis. It should be noted here that both (thin) single- and (thicker) double-epilayer GaAs/Si structures grown on offcut Si substrates show essentially the same general behavior reported above for growth on exactly-oriented Si, and no appreciable differences regarding lattice relaxation state.

The RSM analysis provided a better insight of the microstructure quality and defect properties of GaAs epilayers. Fig. 7 shows the RSMs around the (1 1 1) reciprocal lattice points (rlps) of GaAs and Si recorded for the single- and double-layer samples in Fig. 6. The halo of the (1 1 1) Si rlp (here, defined as the origin for simplicity sake) and (1 1 1)GaAs rlp are clearly observed.

The spacing between the Si and GaAs (1 1 1) rlps are the same for both structures, confirming the relaxed state of the GaAs lattice as observed by DA-axis measurements. However, for the thin single-layer sample the GaAs streak is elongated along the Q_z momentum transfer (i.e., in the direction normal to the crystal surface), while the broadening along the in-plane (Q_x) momentum transfer is very small. On the contrary, the diffuse scattering is much pronounced along the Q_x momentum transfer for the thicker double-layer sample. Line scans along the Q_x and Q_z momentum transfers were extracted from the RSMs: the resulting peaks were then line-shape fitted to estimate the coherence lengths along the two directions (see *Supplementary Information*) and thus the spatial extension of the mosaic blocks constituting the epilayer structure. For the annealed single-layer sample in Fig. 7a the coherence lengths along the in-plane and out-of-plane (growth) directions, L_x and L_z turned out > 500 nm and 5.2 nm, respectively, indicating a platelet-like shape of individual mosaic blocks. The implications of this result are discussed further below. For the double-epilayer sample in Fig. 7b the line scan along Q_x turned out instead, composed of two superposed peak

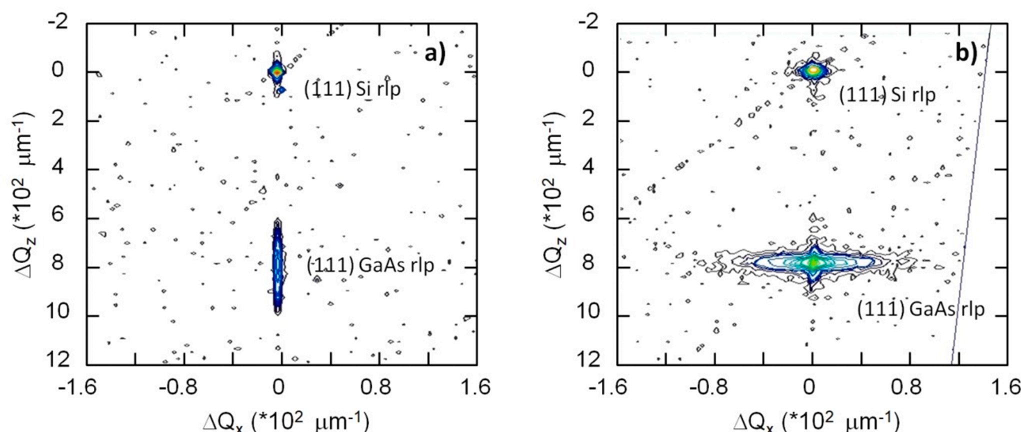

Fig. 7. RSMs around the (1 1 1) rlps of Si and GaAs of (a) single- and (b) double-layer GaAs/Si samples on exactly-oriented (1 1 1)Si (the same intensity scale is used for both maps). The halos around the (1 1 1)GaAs rlp in (a) and (b) are very different, although both layer structures are relaxed with respect to the Si substrate lattice.

Table 1
GaAs coherence lengths along the in-plane and out-of-plane directions, as estimated from line-shape fitting of corresponding RSM line scans of the studied GaAs/Si samples.

Sample type	Si substrate orientation	1st layer annealing	Coherence lengths (nm)				
			1st layer		2nd layer		
			L_x	L_z	L_{x1}	L_{x2}	L_z
Single-layer	exact	NO	>500	3.6	–	–	–
	exact	YES	>500	5.2	–	–	–
	4°-offcut	YES	>200	5.0	–	–	–
Double-layer	exact	YES	*n.d.*	*n.d.*	200	24	31
	exact	YES	*n.d.*	*n.d.*	200	25	32
	4°-offcut	YES	*n.d.*	*n.d.*	145	21	30

contributions with different broadenings (see *Supplementary Information*), leading to L_{x1} ≈200 nm, L_{x2} ≈25 nm and L_z ≈32 nm, respectively. The two in-plane contributions could be ascribed to volumes of different mosaicity composing the GaAs deposit; as a matter of fact, the symmetric DA scan of the double-layer sample in Fig. 6b also shows a GaAs (1 1 1) Bragg peak composed by a broader low intensity peak and a narrower and higher intensity peak. Clearly, these two contributions (not observed in the single-layer samples) both pertain to the second much thicker GaAs layer.

The same analysis has been carried out for several samples deposited on both exactly-oriented and offcut Si wafers (see *Supplementary Information*), as reported in Table 1.. A peculiar behavior could be observed, in regard to as-estimated in-plane and out-of-plane coherence lengths of the samples. As already observed, single-layer samples grown on exactly-oriented Si show quite large (>500 nm) values of the in-plane coherence length L_x. We underline that such value is well above the average size (47.3 nm) of GaAs nanoislands just before coalescence [29], and somewhat larger than the domain size observed in Fig. 1b. However, it agrees fairly well with the estimated average distance between pinholes (i.e., TDs) on the epilayer surface. As it concerns L_z, its values are instead, in the order of a few nm, i.e. much shorter than the GaAs epilayer thickness; Kang *et al.* [22] previously showed by transmission electron microscopy observations that low-temperature grown GaAs thin layers on (1 1 1) Si are affected by stacking faults and micro-twins parallel to the GaAs/Si interface. Our XRD pole figures substantially confirm their finding (A-type twin domains), while present L_z values indicate a micro-twin domain average thickness in the order of 3–5 nm for both exactly-oriented and offcut substrates, despite the lower rotational twin ratio of the latter. As the epilayer in-plane coherence length is likely limited by TDs, L_x represents a lower bound value for the micro-twin in-plane size.

Noteworthy is that the coherence lengths remain almost the same for both as-grown and annealed single-layer samples (see Table 1.), indicating that mutual annealing of dislocations (and possibly of twin domains) goes to completion already during the long low-temperature growth stage. This finding is in apparent contrast with what reported in the literature, i.e. that annealing is necessary to improve the epilayer crystalline quality; however, the result may be a consequence of the very low GaAs growth rates (<0.012 nm/s) during the nucleation stage of our samples with respect to those reported elsewhere (0.03–0.4 nm/s in MBE growth [5,26,37]): indeed, present conditions would favor an epilayer crystallization closer to equilibrium and a better crystal perfection. In this respect, the change of surface morphology observed in Fig. 1 upon sample annealing does not correspond to an epilayer structural improvement, but rather the result of an enhanced mobility of atoms at the epilayer surface. Noteworthy is also that the in-plane coherence length of the single-layer sample grown on the offcut substrate in Table 1. is shorter than that of samples grown on exactly-oriented Si, despite the lower amount of rotational twins observed for the former. This shorter coherence length points out a higher dislocation density for the sample.

As discussed above, the RSMs of the double-layer samples show two superposed contributions to the in-plane diffraction of different intensities and broadening, ascribed to volumes of different mosaicity (i.e., block size) within the top GaAs epilayer. For the two equivalent samples grown on exactly-oriented Si reported in in Table 1., the larger volume blocks return reproducibly an estimated coherence length L_{x1} = 200 nm, while the smaller ones give a length L_{x2} = 24–25 nm; as it regards the out-of-plane diffraction, a single contribution with a coherence length L_z = 31–32 nm is observed. We tentatively ascribe the latter to the same contribution associated with L_{x1}, in reason of its apparently larger overall mosaic volume. We discussed earlier in this work that the estimated rotational twin ratios of double-layer samples are comparable (within experimental uncertainties) to those calculated for single-layer samples: the different coherence lengths reported in Table 1. between the two types of samples, cannot be thus ascribed to a substantial difference in their rotational twin content. Fig. 2 shows that the size of twinned domains in the second epilayer is in the order of a micron, i.e. much larger than the values of L_{x1} and L_{x2} in Table 1., further confirming our conclusion.

As in the case of the single-layer samples, we ascribe the values of L_{x1} and L_z as representative of TD density and micro-twin thickness within the second epilayer, respectively; comparison between figures in Table 1. would then indicate a dislocation density in double-layer samples over 2.5× larger than for the single-layer ones. Indeed, additional dislocations could be ascribed to plastic relaxation of the thermal strain generated upon cooling from the high growth temperature (700 °C) of the double-layer samples. However, more growth experiments are needed to verify whether this is the case, along with the nature of the mosaic contribution associated with L_{x2}. We further evidence that the double-epilayer sample grown on offcut Si shows reduced coherence lengths (in Table 1.) with respect to those grown on exactly-oriented substrates, in analogy with what found for single-epilayer samples on the two type of substrates; clearly, the lower crystalline quality of the first layer affects that of the second one.

Our results show that offcut substrates have a reduced amount of rotational twins, but shorter in-plane coherence lengths, likely associated with higher dislocation densities; at the same time, the lattice tilt of GaAs with respect to Si slightly increases on switching from exactly-oriented to offcut substrates.

In the following, we discuss on the relative roles of substrate offcut and lattice tilt in determining the overall crystalline quality of GaAs epilayers on (1 1 1)Si. Cornet et al. [38] recently studied the impact of substrate offcuts on APD nucleation of III-V/(1 0 0)Si structures, showing that their initial distribution is determined by either a nucleation-driven (for offcut angles typically $> 1°$) or a monolayer terraces-driven (for offcut angles typically $< 0.1°$) regime. In analogy with their nucleation model, one could then speculate whether twinned/untwinned GaAs domain nucleation would be affected (if any) by the monolayer-step distribution across the surface of present Si substrates.

In this respect, the average diameter of our GaAs nano-islands before coalescence is in the 20–47 nm range (depending on the growth time), while their density remains at $\delta \sim 2 \times 10^{10}$ cm^{-2} [29]. Assuming a Poissonian distribution of GaAs nano-island on the Si surface one can

estimate the average distance between neighboring islands along the [11$\overline{2}$] offcut direction $1/\pi\sqrt{\delta} \cong$ 22–23 nm [38]. The distance (terrace length) between monolayer-steps for a 4°-offcut (1 1 1)Si substrate is instead, 4.7 nm. Therefore, both the average distance and nano-island size are much larger than the typical terrace length for our offcut Si substrates. The estimated terrace length for exactly-oriented Si (assuming a substrate orientation error within ±0.5°) is instead ≥ 40 nm (i.e., about 10× that estimated for the offcut substrate), not far from the neighboring nano-island distance estimated above. According to ref. [38], we then estimate a critical offcut angle of 0.08° for the GaAs/(1 1 1)Si system, which would suggest a nucleation-driven regime (or near to) for present samples. However, we like to point here that mono-domain GaAs islands could develop twins (and TBs) as the growth proceeds well before nano-island coalescence, at difference with the case of APDs. The evolution with epilayer growth of twinned domains and their coalescence/annealing cannot thus be described in similarity to APDs as described in ref. [38].

All our samples showed in-plane lengths of the twinned domains in the order of several hundred nm (in Table 1.). In particular, the in-plane coherence lengths of samples grown on offcut Si are not much shorter than that found for exactly-oriented Si, despite the 4.7 nm monolayer terrace length of the former. This finding, together with the reduction of micro-twin concentrations observed for offcut Si substrates, suggests that the surface step density is likely not the main factor affecting the microtwin nucleation; we suggest instead, that lattice registry constrains at the hetero-interface associated with the lattice tilt between GaAs and Si may play a major role: indeed, as larger lattice tilts lead to higher dislocation densities (i.e., plastic relaxation) in our samples, this may in turn rapidly reduce the elastic stress fields within the epilayer, which are the main source of rotational twin nucleation.

4. Conclusions

We reported on the detailed structural characterization of GaAs/(111)Si heteroepitaxial structures double-step grown by MOVPE on both exactly-oriented and offcut (1 1 1)Si substrates. The lattice tilt of GaAs epilayers, their mosaicity and defects content, in particular the types and volume content of rotational twin domains, were determined for the different types of samples (single- and double-layer structures).

Double crystal XRD measurements showed that the epilayers are plastically relaxed and tilted by an angle within the 0.05°−0.08° and 0.11°−0.14° range respectively, for exactly-oriented and offcut substrates; in addition, analysis of XRD pole figures demonstrated the presence of rotational twin domains of different types and orientations. The most abundant ones are originated from a 60°-rotation of the crystal around the [$\overline{1}\overline{1}\overline{1}$] growth direction (A-type rotational twins); rotations around any of the [$\overline{1}11$], [$1\overline{1}1$] and [$\overline{1}1\overline{1}$] equivalent directions, or the composition of a crystal rotation around the growth direction with one of the former (B- and AB-type twins, respectively) were also observed, but having much lower densities. The latter types of twin are reported for the first time in this work.

Annealed single-layer samples grown on exactly-oriented (1 1 1)Si substrates showed the formation of large (sub-micrometric) irregular domains ascribed to GaAs rotational twins and an estimated rotational twin ratio ~ 48%. Furthermore, a large density (~3×10^{8} cm^{-2}) of pinholes were observed across their surface, in numerical agreement with TD densities commonly reported in annealed epilayers of comparable thickness.

Analysis of the sample RSMs allowed to evaluate the epilayer mosaicity and coherence lengths (average dimensions) of crystal blocks/domains along the in-plane and out-of-plane directions. A mosaic of platelet-like shaped blocks was thus identified based on the estimated crystal coherence lengths of the single-layer samples, suggesting that these blocks consist of 3–5 nm thick micro-twin domains parallel to the GaAs/Si interface, their later size (>500 nm) being likely limited by TDs. Noteworthy, the coherence lengths remain almost the same for as-grown and annealed single-layer samples, indicating that the defects reached an equilibrium configuration during the low-temperature growth stage, likely as result of the very low growth rates (<0.012 nm/s) during GaAs nucleation.

The rotational twin ratio estimated for double-layer samples on exactly-oriented Si turned comparable to those of single-layer structures. However, the samples showed two superposed contributions to the in-plane diffraction with different intensities and broadening, ascribed to distinct mosaic block volumes within the top GaAs epilayer. The larger block size has been ascribed to 31–32 nm thick micro-twins parallel to the GaAs/Si hetero-interface, their lateral size (200 nm) being again likely limited by TDs. An increased density of TDs originating from relaxation of thermal strain build-up upon cooling from the higher growth temperature of the second-layer could be at the origin of this effect. The second contribution to mosaicity, arises instead from smaller blocks with in-plane average size around 24–25 nm, whose nature requires however, further studies.

Finally, the double-layer samples grown on offcut (1 1 1)Si showed reduced coherence lengths (reduced mosaic block size) with respect to those on exactly-oriented substrates, the lateral size of their larger mosaic blocks being 200 nm; the rotational twin content also decreases to 32%. These results confirm the trend observed for single-epilayer samples, indicating that while GaAs epilayers grown on offcut Si tend to be less prone to twin nucleation, they show a larger dislocations density. We finally suggest that lattice registry constrains at the hetero-interface, associated with the lattice tilt between GaAs and Si, play a major role in determining the defect types and content in as-grown epilayers.

Present results contribute to deeper understand the crystalline properties of GaAs epilayers on (1 1 1)Si and their change with growth/annealing conditions and surface-cutting of the Si substrate.

CRediT authorship contribution statement

Nico Lovergine: Investigation, Visualization, Conceptualization, Writing – original draft, Writing – review & editing, Funding acquisition. **Ilio Miccoli:** Investigation, Visualization, Writing – original draft. **Leander Tapfer:** Investigation, Visualization, Writing – review & editing. **Paola Prete:** Investigation, Resources, Funding acquisition, Supervision, Writing – review & editing.

Declaration of Competing Interest

The authors declare that they have no known competing financial interests or personal relationships that could have appeared to influence the work reported in this paper.

Data availability

Data will be made available on request.

Acknowledgements

The authors would like to acknowledge F. Marzo for assistance during MOVPE growth and FESEM observations. D. Cannoletta is also thanked for his valuable help during XRD pole figure measurements.

Appendix A. Supplementary material

Supplementary data to this article can be found online at https://doi.org/10.1016/j.apsusc.2023.157627.

References

[1] D. Liang, J.E. Bowers, Recent progress in lasers on silicon, Nat. Photonics 4 (2010) 511–517, https://doi.org/10.1038/nphoton.2010.167.

[2] B. Shi, B. Song, A.A. Taylor, S.S. Brunelli, J. Klamkin, Selective area heteroepitaxy of low dislocation density antiphase boundary free GaAs microridges on flat-bottom (001) Si for integrated silicon photonics, Appl. Phys. Lett. 118 (2021), 122106, https://doi.org/10.1063/5.0043027.

[3] K.N. Yaung, M. Vaisman, J. Lang, M.L. Lee, GaAsP solar cells on GaP/Si with low threading dislocation density, Appl. Phys. Lett. 109 (2016), 032107, https://doi.org/10.1063/1.4959825.

[4] M. Vaisman, S. Fan, K.N. Yaung, E. Perl, D. Martín-Martín, Z.J. Yu, M. Leilaeioun, Z.C. Holman, M.L. Lee, 15.3%-efficient GaAsP solar cells on GaP/Si templates, ACS Energy Lett 2 (2017) 1911–1918, https://doi.org/10.1021/acsenergylett.7b00538.

[5] V. Alberts, J.H. Neethling, J.S. Vermaak, Nucleation and growth of gallium arsenide on silicon (111), J. Mater. Sci. 29 (1994) 2017–2024, https://doi.org/10.1007/BF01154676.

[6] Y.B. Bolkhovityanov, O.P. Pchelyakov, GaAs epitaxy on Si substrates: modern status of research and engineering, Phys.-Usp. 51 (5) (2008) 437–456, https://doi.org/10.1070/PU2008v051n05ABEH006529.

[7] C. Koppka, A. Paszuk, M. Steidl, O. Supplie, P. Kleinschmidt, T. Hannappel, Suppression of rotational twin formation in virtual GaP/Si(111) substrates for III−V nanowire growth, Cryst. Growth Des. 16 (2016) 6208–6213, https://doi.org/10.1021/acs.cgd.6b00541.

[8] A. Navarro, E. García-Tabarés, Q.M. Ramasse, P. Caño, I. Rey-Stolle, B. Galiana, Advanced transmission electron microscopy investigation of defect formation in MOVPE-growth of GaP on silicon using arsenic initial coverage, Appl. Surf. Sci. 610 (2023) 155578,, https://doi.org/10.1016/j.apsusc.2022.155578.

[9] Q. Li, K.M. Lau, Epitaxial growth of highly mismatched III-V materials on (001) silicon for electronics and optoelectronics, Progr. Cryst. Growth Character. Mater. 63 (2017) 105–120, https://doi.org/10.1016/j.pcrysgrow.2017.10.001.

[10] O. Supplie, O. Romanyuk, C. Koppka, M. Steidl, A. Nägelein, A. Paszuk, L. Winterfeld, A. Dobrich, P. Kleinschmidt, E. Runge, T. Hannappel, Metalorganic vapor phase epitaxy of III–V-on-silicon: experiment and theory, Progr. Cryst. Growth Character. Mater. 64 (2018) 103–132, https://doi.org/10.1016/j.pcrysgrow.2018.07.002.

[11] W. Stolz, Y. Horikoshi, M. Naganuma, K. Nozawa, Optimized growth start and controlled formation of misfit dislocations for eteroepitaxial GaAs on (100) Si grown by migration-enhanced epitaxy, J. Cryst. Growth 95 (1989) 87–90, https://doi.org/10.1016/0022-0248(89)90357-6.

[12] Q. Li, H. Jiang, K.M. Lau, Coalescence of planar GaAs nanowires into strain-free three dimensional crystals on exact (001) silicon, J. Cryst. Growth 454 (2016) 19–24, https://doi.org/10.1016/j.jcrysgro.2016.08.051.

[13] B. Shi, A. Goswami, A.A. Taylor, S.T. Suran Brunelli, C. Palmstrøm, J. Klamkin, Antiphase boundary free InP microridges on (001) silicon by selective area heteroepitaxy, Cryst. Growth Des. 20 (2020) 7761–7770, https://doi.org/10.1021/acs.cgd.0c00988.

[14] B. Mayer, D. Rudolph, J. Schnell, S. Morkötter, J. Winnerl, J. Treu, K. Müller, G. Bracher, G. Abstreiter, G. Koblmüller, J.J. Finley, Lasing from individual GaAs-AlGaAs core-shell nanowires up to room temperature, Nat. Commun. 4 (2013) 2931, https://doi.org/10.1038/ncomms3931.

[15] E.M. Gallo, G. Chen, M. Currie, T. McGuckin, P. Prete, N. Lovergine, B. Nabet, J. E. Spanier, Picosecond response times in GaAs/AlGaAs core/shell nanowire-based photodetectors, Appl. Phys. Lett. 98 (2011), 241113, https://doi.org/10.1063/1.3600061.

[16] A. Persano, B. Nabet, A. Taurino, P. Prete, N. Lovergine, A. Cola, Polarization anisotropy of individual core/shell GaAs/AlGaAs nanowires by photocurrent spectroscopy, Appl. Phys. Lett. 98 (2011), 153106, https://doi.org/10.1063/1.3578189.

[17] A. Cretì, P. Prete, N. Lovergine, M. Lomascolo, Enhanced optical absorption of GaAs near-band-edge transitions in GaAs/AlGaAs core–shell nanowires: Implications for nanowire solar cells, ACS Appl. Nano Mater. 5 (2022) 18149–18158, https://doi.org/10.1021/acsanm.2c04044.

[18] P. Prete, N. Lovergine, Dilute nitride III-V nanowires for high-efficiency intermediate-band photovoltaic cells: materials requirements, self-assembly methods and properties, Progr. Cryst. Growth Character. Mater. 66 (2020), 100510, https://doi.org/10.1016/j.pcrysgrow.2020.100510.

[19] D. Wolf, R. Hübner, T. Niermann, S. Sturm, P. Prete, N. Lovergine, B. Büchner, A. Lubk, Three-dimensional composition and electric potential mapping of III−V Core−multishell nanowires by correlative STEM and holographic tomography, Nano Lett. 18 (2018) 4777–4784, https://doi.org/10.1021/acs.nanolett.8b01270.

[20] G. Koblmüller, B. Mayer, T. Stettner, G. Abstreiter, J.J. Finley, GaAs−AlGaAs core−shell nanowire lasers on silicon: Invited review, Semicond. Sci. Technol. 32 (2017), 053001, https://doi.org/10.1088/1361-6641/aa5e45.

[21] I. Miccoli, P. Prete, F. Marzo, D. Cannoletta, N. Lovergine, Vertically-aligned GaAs nanowires on GaAs/(111)Si heterosubstrates by metalorganic vapour phase epitaxy, Cryst. Res. Technol. 46 (8) (2011) 795–800, https://doi.org/10.1002/crat.201000711.

[22] J.H. Kang, Q. Gao, H.J. Joyce, H.H. Tan, C. Jagadish, Y. Kim, D.Y. Choi, Y. Guo, H. Xu, J. Zou, M.A. Fickenscher, L.M. Smith, H.E. Jackson, J.M. Yarrison-Rice, Novel growth and properties of GaAs nanowires on Si substrates, Nanotechnol. 21 (2010), 035604, https://doi.org/10.1088/0957-4484/21/3/035604.

[23] H.A. Fonseka, H.H. Tan, J. Wong-Leung, J.H. Kang, P. Parkinson, C. Jagadish, High vertical yield InP nanowire growth on Si(111) using a thin buffer layer, Nanotechnol. 24 (2013), 465602, https://doi.org/10.1088/0957-4484/24/46/465602.

[24] G. Chen, E.M. Gallo, J. Burger, B. Nabet, A. Cola, P. Prete, N. Lovergine, J. E. Spanier, On direct-writing methods for electrically contacting GaAs and Ge nanowire devices, Appl. Phys. Lett. 96 (2010), 223107, https://doi.org/10.1063/1.3441404.

[25] H. Suzuki, D. Ito, A. Fukuyama, T. Ikari, Reduction of rotational twin formation by indium pre-evaporation in epitaxially grown GaAs films on Si (111) substrate, J. Cryst. Growth 380 (2013) 148–152, https://doi.org/10.1016/j.jcrysgro.2013.06.015.

[26] P. Vennéguès, L. Largeau, V. Brändli, B. Damilano, K. Tavernier, R. Bernard, A. Courville, S. Rennesson, F. Semond, G. Feuillet, C. Cornet, On the origin of twist in 3D nucleation islands of tetrahedrally coordinated semiconductors heteroepitaxially grown along hexagonal orientations, J. Appl. Phys. 132 (2022), 165102, https://doi.org/10.1063/5.0111558.

[27] A. Proessdorf, M. Hanke, B. Jenichen, W. Braun, H. Riechert, Volmer-Weber growth of AlSb on Si(111), Appl. Phys. Lett. 102 (2013), 041601, https://doi.org/10.1063/1.4789536.

[28] I. Lucci, S. Charbonnier, L. Pedesseau, M. Vallet, L. Cerutti, J.-B. Rodriguez, E. Tournié, R. Bernard, A. Létoublon, R. Bertru, A. Corre, S. Rennesson, F. Semond, G. Patriarche, L. Largeau, P. Turban, A. Ponchet, C. Cornet, Universal description of III-V/Si epitaxial growth processes, Phys. Rev. Mater. 2 (2018), https://doi.org/10.1103/PhysRevMaterials.2.060401, 060401(R).

[29] I. Miccoli, P. Prete, N. Lovergine, Shape size evolution and nucleation mechanisms of GaAs nanoislands grown on (111)Si by low temperature metalorganic vapor phase epitaxy, Cryst. Growth Des. 19 (2019) 5523–5530, https://doi.org/10.1021/acs.cgd.9b00225.

[30] J.R. Patel, P.E. Freeland, M.S. Hybertsen, D.C. Jacobsen, J.A. Golovchenko, Location of atoms in the first monolayer of GaAs on Si, Phys. Rev. Lett. 59 (1987) 2180–2183, https://doi.org/10.1103/PhysRevLett.59.2180.

[31] A. Strömberg, P. Bhargava, Z. Xu, S. Lourdudoss, Y.-T. Sun, Direct heteroepitaxy and selective area growth of GaP and GaAs on Si by hydride vapor phase epitaxy, Phys. Status Solidi A 218 (2021) 2000447, https://doi.org/10.1002/pssa.202000447.

[32] A. Hangleiter, F. Hitzel, C. Netzel, D. Fuhrmann, U. Rossow, G. Ade, P. Hinze, Suppression of nonradiative recombination by V-shaped pits in GaInN/GaN quantum wells produces a large increase in the light emission efficiency, Phys. Rev. Lett. 95 (2005), 127402, https://doi.org/10.1103/PhysRevLett.95.127402.

[33] D. Gerthsen, F.A. Ponce, G.B. Anderson, H.F. Chung, Lattice mismatch effects in GaAs epitaxy on Si and GaP, Mater. Res. Soc. Symp. Proc. 122 (1988) 21–26, https://doi.org/10.1557/PROC-122-21.

[34] C. Lin, M.M. Fejer, J.S. Harris, Antiphase domain annihilation during growth of GaP on Si by molecular beam epitaxy, J. Cryst. Growth 363 (2013) 258–263, https://doi.org/10.1016/j.jcrysgro.2012.10.055.

[35] L. De Caro, C. Giannini, L. Tapfer, Determination of the lattice strain and chemical composition of semiconductor heterostructures by high-resolution x-ray diffraction, J. Appl. Phys. 79 (1996) 4101–4110, https://doi.org/10.1063/1.361773.

[36] L. Tapfer, J.R. Martinez, K. Ploog, Structural investigation by X-ray diffraction of GaAs epilayers and AlAs/GaAs superlattices grown on <100>Si by MBE, Semicond. Sci. Technol. 4 (1989) 617–621, https://doi.org/10.1088/0268-1242/4/8/003.

[37] Z. Sobiesierski, D.A. Woolf, D.I. Westwood, R.H. Williams, Photoluminescence measurements for GaAs grown on Si(100) and Si(111) by molecular beam epitaxy, Appl. Phys. Lett. 58 (1991) 628–630, https://doi.org/10.1063/1.104550.

[38] C. Cornet, S. Charbonnier, I. Lucci, L. Chen, A. Létoublon, A. Alvarez, K. Tavernier, T. Rohel, R. Bernard, J.-B. Rodriguez, L. Cerutti, E. Tournié, Y. Léger, M. Bahri, G. Patriarche, L. Largeau, A. Ponchet, P. Turban, N. Bertru, Zinc-blende group III-V/group IV epitaxy: importance of the miscut, Phys. Rev. Materials 4 (2020), 053401, https://doi.org/10.1103/PhysRevMaterials.4.053401.

[39] P. Prete, D. Wolf, F. Marzo, N. Lovergine, Nano-scale spectroscopic imaging of GaAs-AlGaAs quantum well tube nanowires: Correlating luminescence with nanowire size and inner multi-shell structure, Nanophotonics 8 (2019) 1567–1577, https://doi.org/10.1515/nanoph-2019-0156.